Temporal and Spatial Deep Learning Network for Infrared Thermal Defect Detection

Qin Luo[1], Bin Gao[1*], W.L. Woo[2], Yang Yang[3]

[1]School of Automation, University of Electronic Science and Technology of China, China

[2]Department of Computer and Information Science, Northumbria University, England, UK

[3]Chengdu aircraft industry Co., Ltd.

*Corresponding author: bin_gao@uestc.edu.cn

Abstract: Most common types of defects for composite are debond and delamination. It is difficult to detect the inner defects on a complex shaped specimen by using conventional optical thermography nondestructive testing (NDT) methods. In this paper, a hybrid of spatial and temporal deep learning architecture for automatic thermography defects detection is proposed. The integration of cross network learning strategy has the capability to significantly minimize the uneven illumination and enhance the detection rate. The probability of detection (POD) has been derived to measure the detection results and this is coupled with comparison studies to verify the efficacy of the proposed method. The results show that visual geometry group-Unet (VGG-Unet) cross learning structure can significantly improve the contrast between the defective and non-defective regions. In addition, investigation of different feature extraction methods in which embedded in deep learning is conducted to optimize the learning structure. To investigate the efficacy and robustness of the proposed method, experimental studies have been carried out for inner debond defects on both regular and irregular shaped carbon fiber reinforced polymer (CFRP) specimens.

Key words: deep learning, segmentation, thermography defect detection, Nondestructive Testing

1 Introduction

Composite materials are important structural materials in which has been widely used in aerospace, wind turbine blades and etc. The defects produced during manufacture and in-service of laminated composites lead to potential safety hazard to the device as well as resulting in immeasurable losses [1]. Therefore, non-destructive testing and evaluation (NDT&E) is the key technology to guarantee the quality of major construction equipment manufacturing and operation safety.

At present, different NDT&E technology has been used to assess the internal quality of CFRP such as penetrant testing (PT), eddy current testing (ECT), ultrasonic testing (UT), and infrared thermography (IT) [2]. Compared with traditional detection technology, optical pulsed thermography (OPT) has the advantages of large single detection area, fast speed, non-contact, field application, safety and simple operation [3]. In recent years, it has been widely studied in the field of NDT&E for composite materials, and gradually become an important means to analyze the failure reasons.

Thermal images using the OPT system suffer from edge blurring, uneven heating and low resolution. In order to solve the above problems, different feature extraction algorithms are applied. Principal component analysis algorithm (PCA) is a commonly used algorithm for extracting defect information in time series [4]. In combing both spatial and temporal information, PCA enhances the detectability of singular regions [5]. Thermographic

signal reconstruction (TSR) [6] eliminates high frequency noise and enhances the visibility of defects by approximate the temperature evolution at each pixel in n-degree polynomial function. Finally, n+1 frame images are reconstructed from the polynomial coefficients. Hajrya R *et al.* [7] applied independent component analysis (ICA) in health structure monitoring. It analyzed the symmetric matrix obtained from the hybrid matrix, and defined the damage index (DI). Cheng L *et al.* [8] combined PCA and ICA to highlight abnormal patterns while extracting orthogonal heat map features. Pulsed phase thermography (PPT) [9-10] is a method for transforming time domain features into frequency domain, extracting defect information from frequency domain information, and eliminating noise. According to the sparsity characteristic of the infrared heat map with defects, Gao B *et al.* [11-13] proposed an adaptive variational Bayesian method. These methods assume that the defect areas are sparse distributed and the background is low rank matrix. The detection of these methods yields high-accuracy objective performance in extracting sparse component after separating the background. Pilla.M *et al*. [14] improved the signal-to-noise ratio of the signal and better obtain the defect information by using the absolute value contrast algorithm. V.P. Vavilov *et al*. [15] obtained defect information by analyzing the value of the surface pixel temperature. Zheng K et al.[16-17] have done in-depth research on the removal of non-uniform background, and the proposed algorithm can effectively reduce noise and enhance image contrast. Wang J G at al. [18] use the method of wavelet transform to denoise the image and improve the SNR value. Venegas P et al. [19] synthesize sequences into a RGB image to speed up the detection. Wang J et al. [20] considers the spatial relationship between pixels, and proposes a method based on region to locate defects. Liu Y et al. [21] use manifold learning thermography (MLT) and isometric feature mapping ((ISOMAP) to distinguish different regions of the thermal images, which improves the detection rate of defects. In terms of infrared image segmentation, Du Feng *et al.* [22] proposed infrared image segmentation based on the index of entropy maximization of the 2-D grayscale histogram. Mei Lin *et al*. [23] focused on the correction of infrared images under non-uniform heating conditions and the problem of defect segmentation with different local contrast. Gao B *et al.* [24] proposed an automatic selection of region growth method, which has obtained good results in aerospace composites. Cluster-based segmentation method [25] is also applied to the detection of defects. Yousefi B et al. [26] combine sparse principal component analysis (SPCA) with K-means clustering to achieve automatic segmentation of defects. In order to avoid the possibility of losing necessary defect information, Zheng K et al. [27-28] analysis all the thermographic data. The thermographic cluster analysis (TCA) method and hyper-image segmentation method can automatically segment the shape of the defect. Gao B et al. [29] use the first-order statistics of genetics to to quantitatively segment defects.

Image segmentation algorithms have been widely used in natural image processing whereas they are rarely applied in infrared thermography nondestructive testing. Consequently, the application of segmentation deep learning networks in the infrared thermal image NDT is a noteworthy direction. Originally, the image block classification method is commonly used where each pixel is divided into the corresponding categories by using image blocks. The main reason for using image blocks is that the classification network usually has a fully connected layer whose input needs to be a fixed size image block. Visual geometry group (VGG) is a convolutional neural network (CNN) model introduced by the visual geometry group and one of the structures is composed by 16 weight layers. It is using smaller filter sizes and spacing on the first volume base layer in which leads to less parameters and more nonlinearities [30]. In 2015, Fully convolutional networks (FCN) is proposed where this is [31] extended from the original CNN structure to an enable intensive prediction without a fully connected layer. This structure allows the segmentation map to generate images of any size, and improves the processing speed. Badrinarayanan *et al*. [32] proposed a deep convolutional encoder-decoder structure for image segmentation-Segnet. The FCN network replicates the characteristics of the encoder, and Segnet transfers the maximum pooling index to the decoder, which is more efficient in memory usage and improves the partition

resolution. In 2015, Fisher Yu *et al*. [33] proposed dilated convolutions for multi-scale aggregation, which increased the receptive field and benefits the classification network. It is a convolutional layer that can be used for dense prediction. However, the computational cost is relatively high, and a large number of high-resolution feature maps need to be processed in which consumes a large amount of memory. In 2016, Liang-Chieh Chen *et al*. [34] proposed DeepLab which implements atrous spatial pyramid pooling (ASPP) in spatial dimension and uses fully connected conditional random fields. Guosheng Lin *et al*. [35] proposed RefineNet as all components follow the design of the residual connection, and the encoder is ResNet-101 [36] module. Hengshuang Zhao *et al*. [37] proposed PSPNet which using the pyramid pooling module to aggregate background information. The pyramid pooling module in the ResNet network adds additional losses in addition to the loss of the main branch. Olaf Ronneberger *et al*. [38] proposed a network structure of encode-decoder, U-net. In this network, the encoder gradually reduces the spatial dimension of the pooling layer, and the decoder gradually repairs the details and spatial dimensions of the object. This network is proved to have good performance in small sample sets.

Although unsupervised learning method has made considerable research progress in thermography processing, the commonly used detection algorithms still have limitations in defect extraction due to weak signals, complex interference and etc. Based on the spatial-temporal physic characteristics of the infrared sequences, the construction of supervised learning to study the infrared non-destructive testing in segmentation networks is a potential trend. This study investigates the performance of several typical deep learning networks on the segmentation of optically excited infrared heat map defects. Particularly, the integration of cross network learning strategy is proposed to significantly minimize uneven illumination and enhance the detection rate. Notwithstanding above, all different algorithms are detail discussed in enhancing detection contrast from the spatial and the temporal domain, respectively. The effects of data enhancement and different preprocessing methods on defect segmentation are investigated as well.

The rest of the paper is organized as follows: Section II describes the basic theory of the OPT system and the deep learning structure for thermography NDT. Section III introduces the design of the experiment and analyses the results. Section IV concludes the study and outlines the future work.

2 Methodology

2.1 Introduction of OPT

Optical pulsed thermography combing light and thermal imaging technology in which can achieve rapidly detection of a wide range for inner defects. OPT is based on the principle of heat conduction. When uniform light is irradiated onto the surface of the specimen, the object absorbs the energy of the incident light and converts it into heat energy, which then form a heat distribution. If there exists a defect in the specimen, it will cause the heat to be uneven and reflected directly on the surface of the specimen. IR camera can be used to record both the spatial and the transient response of the temperature on the sample. Fig.1 shows a diagram of the OPT system composition by using halogen lamps as excitation source.

In OPT system, the temperature field of the measured object can be expressed as a function of spatial and transient by using a mathematical model:

$$T = f(x, y, z, t) \tag{1}$$

The process of heat wave propagation in the medium follows the heat conduction equation. Assuming that the thermal conductivity is a constant, the heat conduction equation can be expressed as:

$$\frac{\partial T}{\partial t}=\frac{k}{\rho C_p}\left(\frac{\partial^2 T}{\partial x^2}+\frac{\partial^2 T}{\partial y^2}+\frac{\partial^2 T}{\partial z^2}\right)+\frac{q}{\rho C_p} \quad (2)$$

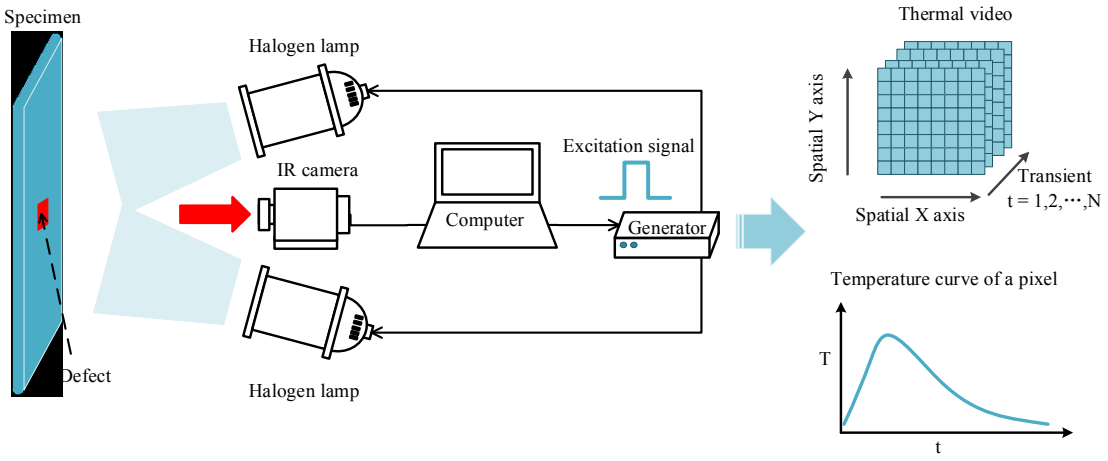

Fig.1. Diagram of OPT system and thermal data

where k denotes the thermal conductivity of the material, ρ is the density of the material, C_p is the specific heat capacity, q is the heat generation per unit volume, which is caused by light excitation. The speed at which heat propagates through the material can be expressed as thermal diffusivity by α :

$$\alpha=\frac{k}{\rho c_p} \quad (3)$$

Bring equation (3) into (1), then (1) can be rewritten as:

$$\frac{\partial T}{\partial t}=\alpha\left(\frac{\partial^2 T}{\partial x^2}+\frac{\partial^2 T}{\partial y^2}+\frac{\partial^2 T}{\partial z^2}+\frac{q}{k}\right) \quad (4)$$

It can be seen that the bigger α is, the faster the temperature changes. For a planar pulsed heat source, since the process reach the end of the heating at the cooling phase, in which non heat is generated per volume (q=0), its ideal one-dimensional mechanism can be expressed by equation (5)

$$\frac{\partial T}{\partial t}=\alpha\frac{\partial^2 T}{\partial z^2} \quad (5)$$

In practical applications, only the surface temperature can be obtained by IR camera, that is z = 0. If there is a defect with a depth of d in the specimen, the heat wave will be blocked and reflected. The surface temperature and the surrounding thermal pattern will be inconsistent. Thus, the defect and abnormality can be identified by the infrared heat map.

2.2 Temporal and Spatial Deep Learning Network for OPT Defect Detection

This section proposes a comparative strategy for segmenting debonded specimens by investigating different deep learning networks. Based on the above analysis, two types of networks will be considered as the characteristic of spatial and temporal information. The main comparative strategy can be summarized as the following four stages: data collecting of a sequence of temperature images (Stage I), data preparation and manual labeling for train and test (Stage II), investigating of different segmentation method by constructing deep learning or cross learning techniques (Stage III), quantitative evaluation for the result of the method (Stage IV).

The whole strategy can be shown in Fig.2.

Given the thermal image sequence of the sample with inner defects, the image sequence can be segmented by using a deep learning method. In this paper, the segmentation results of different deep learning networks on the OPT thermal video will be compared from the aspects of both spatial and temporal domain. In particular, an integration of cross network learning strategy is proposed to enhance the performance. In addition, the investigation of the production and preprocessing of the data sets, different deep learning models and quantitative evaluation methods will be discussed.

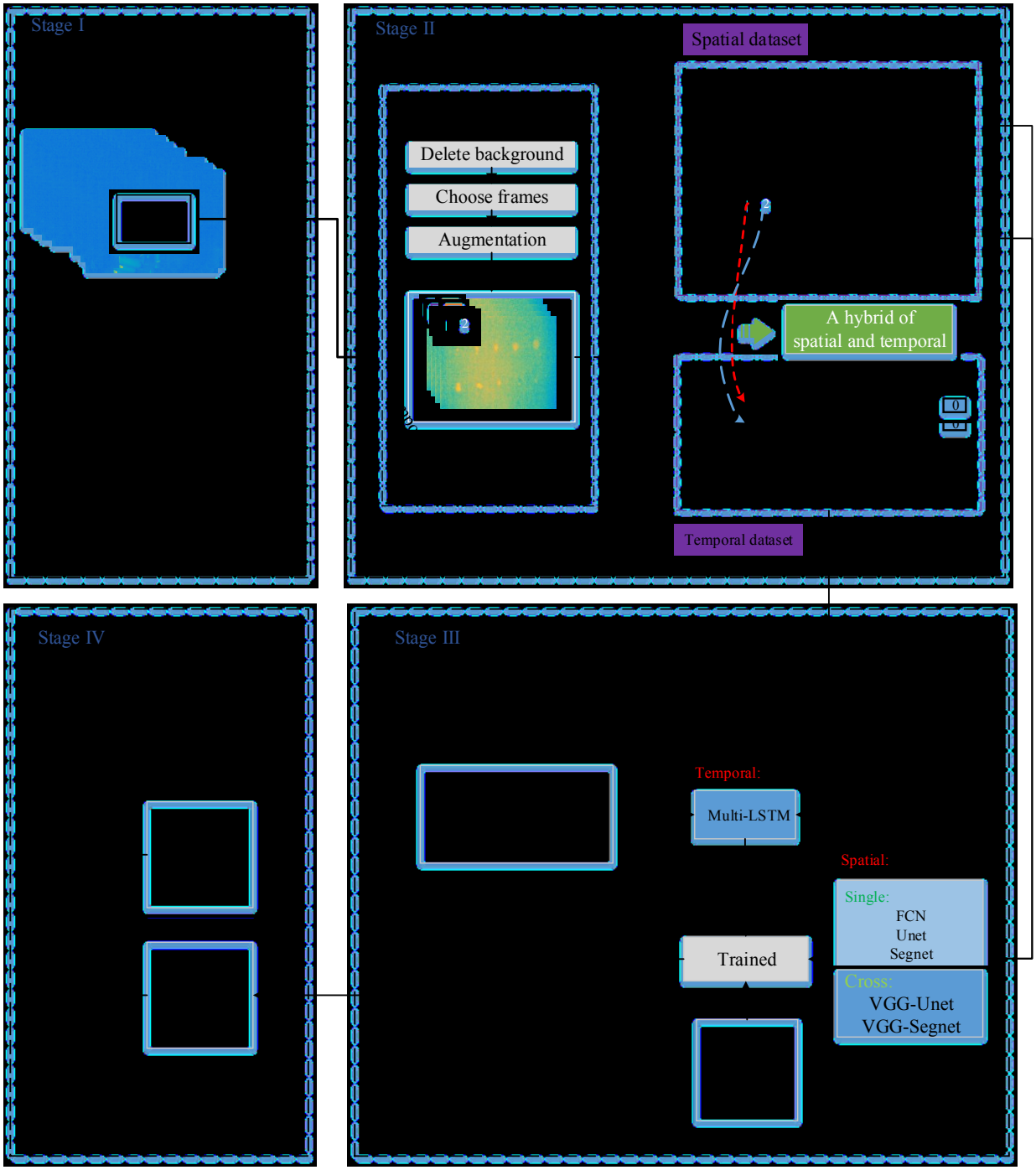

Fig.2. Proposed strategy for segmentation of defect detectability

2.2.1 Thermal spatial characteristic in deep learning structure

According to the principle of heat conduction, when there exists a defect in the internal structure of the object (for example, debonding), the diffusion and transmission of the heat flow are affected. This effect is manifested by the difference in temperature at the surface of the object, which in turn causes an abnormality in the observed distribution. Fig.3 shows the temperature distribution on the surface of the object in the presence or absence of defects inside. The temperature distribution on the surface of non-defect homogeneous specimen is depicted in figure (a) and (d). When the incident wave is partially reflected on the surface of the material, the other parts will continue to propagate downward, a uniform temperature field is formed on the surface. In figure (b) and (e), since the thermal conductivity of the defective region is smaller than other regions of the material, the downward propagation of the incident wave at the defect position is hindered, and the reflected wave is increased, so that a hot region is formed on the surface of the specimen. On the contrary, for the thermal conductivity defect, since the thermal conductivity of the defect is smaller, the reflected wave of the area is reduced and a cold zone is formed on the surface. The details are shown in figure (c) and (f). The properties of this hot zone and cold zone can be used in space model to detect defects.

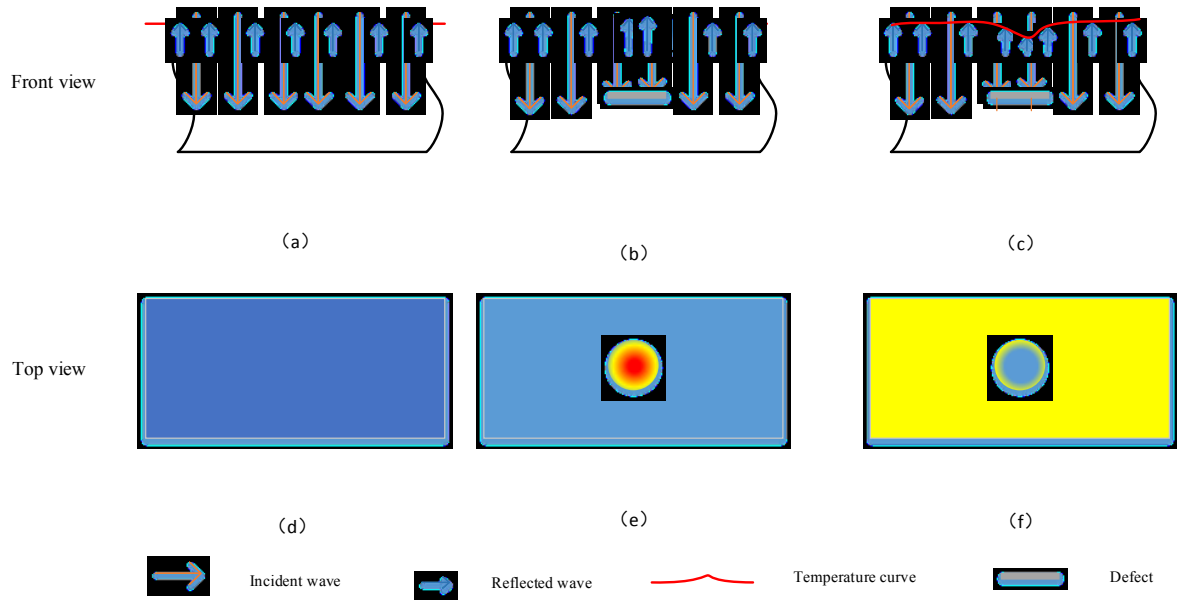

Fig. 3. Surface temperature field distribution under different conditions: (a) (d): homogeneous; (b) (e): thermal insulation defect; (c) (f): thermal conductivity defect.

Taking the thermal insulation defect as an example, each thermal frame of size $m \times n$ is represented by *X*, which required to segment defects. it is assumed that the defect feature (hot zone) is the foreground represented by D, the non-defect feature (cold zone) is a background as represented by S. The uneven heating due to material properties and heating conditions can be regarded as noise as represented by N. Thus, each thermal frame can be expressed by:

$$X = D + S + N \tag{6}$$

For each specimen, the ground-truth label image Y that is calibrated according to the actual defect position and size is defined as a binary map, where zeros and ones represent sound and defective areas respectively.

In the field of semantic segmentation, certain deep networks have made such significant contributions to the field that they have become widely known standards, such as the fully convolutional network (FCN), Unet, Segnet. All these spatial-type based deep learning networks have achieved good results in natural image

segmentation. Exploring the application of deep learning networks in OPT is one of the goals. The spatial models are all encoder-decoder models. The output of the model can be expressed as (7), where $\hat{Y}$ is an image predicted by the model, and W is the weight of X. In the encoder stage, different features such as noise, defects, and defect edges can be extracted through different kernels. In the training process, adjust the weight W of different features to make $\hat{Y}$ closer to Y adaptively through the guidance of the label, and finally the focus of the network will fall on the defect.

$$\hat{Y} = WX + b \tag{7}$$

The model is going to conduct optimization by reducing the error between Y and $\hat{Y}$. Binary cross entropy is used to this loss function as defined as:

$$L = -\frac{1}{N}\sum_{i=1}^{m\times n}(y_i \log \hat{y}_i + (1-y_i)\log(1-\hat{y}_i)) \tag{8}$$

where $N = m \times n$ is the total number of pixels, y_i is the binary value corresponding to i in the label Y. $\hat{y}_i$ is the predicted probability of the pixel.

For the encoder-decoder model, they can capture several basic information of the tested object, such as background noise, texture, and shape etc., in the first few layers of the encoder. Advanced information will be extracted in the following deep layers. Compared with FCN, the large changes in structure of Unet are decoder phase. An upsampling layer is added after each convolutional layer to increase the resolution of the image in decoder. The convolution operation is performed on the layer to impose a high dimensional feature. As shown in Fig.4, in the decoding process, in order to emphasis the high-resolution features, the feature map of the encoder is connected to the upsampled feature map. Under the guidance of labels and high-resolution features, the model can learn more accurate shape, size and localization information of defects through multiple iterations. At the same time, the edge of the defect is more obvious and the influence of the heat diffusion is getting weakened. In this paper, batch normalization and dropout are applied to improve model accuracy and reduce overfitting.

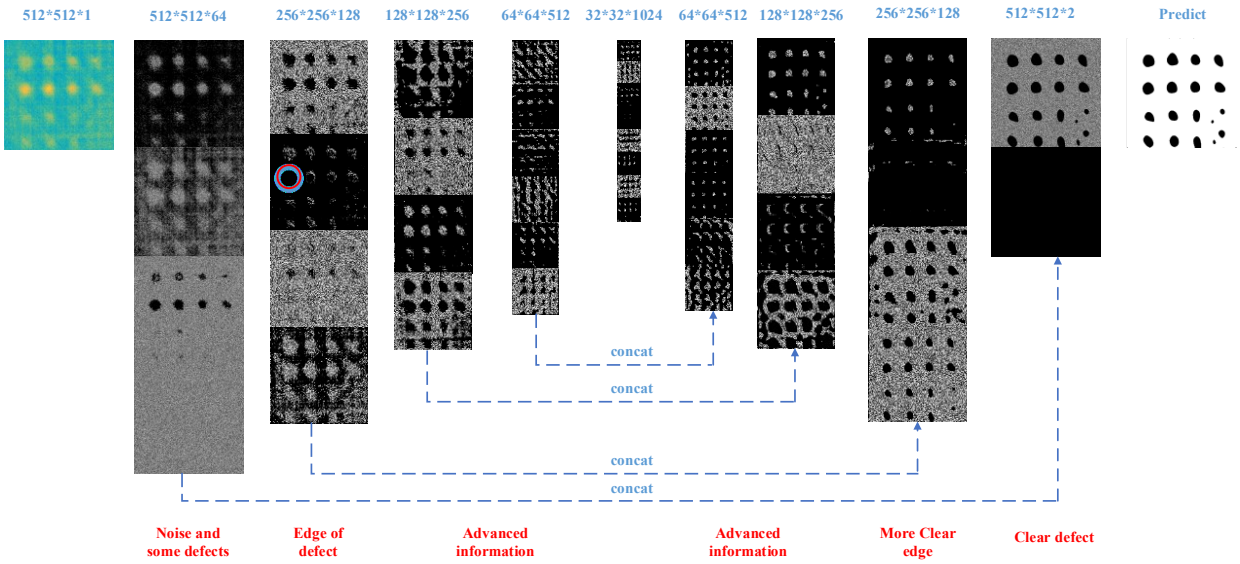

Fig.4. Structure of spatial model

The generation of the training dataset is also a key condition for the model to be effective. The data process of the spatial model is explained below.

It is divided into two parts: the selection of the training data and the calibration of the data (labeling).

a)：selection of training data

The training set contains four different types of specimens, each specimen contains the defects with different diameters and depths. For the obtained image sequence, 50 frames with higher contrast in the t-m~t+m-1 frames are extracted, where t is the highest temperature frame and m is a multiple of 25. The temperature gap between the defect area and the non-defect area is the largest around the frame with the highest temperature, which is more conducive to the segmentation of the defect by the model. This can be explained by thermal temporal characteristic of the heat conduction. The first frame is subtracted to remove the background noise, and then the environmental background around the specimen is cut, now the original dataset A is obtained.

Data augmentation is essential to guide the network to obtain the desired invariance and robustness properties since only few training samples are available. Therefore, methods such as color conversion and rotation are used to augment the data, namely dataset B.

b): calibration of the data

For the supervision learning, corresponding labels for the above training data are required to generate. Since the position of the specimen is fixed during the experiment and the relative position of the defect does not change with time, each thermal sequence uses a same label. The label making process for each specimen is shown in Fig.5：a) Select one frame with the strongest defect information in the thermal sequence confirmed by peers and preparation map; b) Use the data calibration tool - *labelme* to calibrate the defects of the frame image. The process will be confirmed by multiple peers; c) generate a binary image.

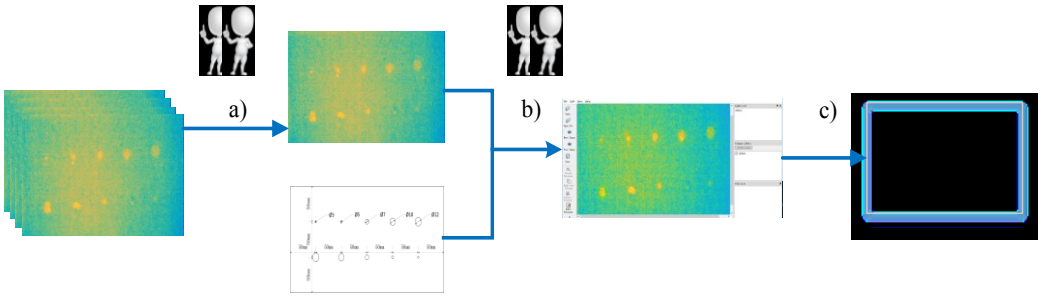

Fig.5. Process of labeling

2.2.2 Thermal temporal characteristic in deep learning structure

From the perspective of the entire inspection process, temporal behavior of the surface temperature for defect and sound area is different. This is shown in Fig.6. For the insulation defect, in the heating stage, the temperature of the defect area rises rapidly, and the sound area rises slowly. Therefore, a temperature gap is formed. Especially in the vicinity of the end of heating, the difference in temperature time curves between the two regions is more pronounced. It is worth noting that the change of the surface temperature of the test piece is a continuous process, and the temperature of each frame collected by the infrared camera is related to its historical frames that the closer to that moment, the greater the impact. This feature can be applied to time series prediction model with memory. In the sequence model, long short term memory (LSTM) is such an excellent time-series network that can handle continuous information, and it solves the long-term dependence of recurrent neural network (RNN), that is, the information required to predict the result is lost due to the long interval. For each pixel of a frame, a temperature change curve over time can be obtained on the given image sequence. According to the temperature change of each pixel, the time series model can distinguish whether the pixel belongs to a defective area or a sound area.

A 3-layer long short term memory (3-layer LSTM) loop is applied to capture the physical properties that mining the feature of the temperature varies between the defect point and the non-defect point. The process of

3-layer-LSTM segmentation is shown in Fig.7. The obtained thermal video data is de-background and normalized, and n-frame data of a fixed duration is selected as the preprocessed data. Each pixel is vectorized in time, and then the vectorized data is input into the 3-layer LSTM. The predicted value of the model for this pixel sequence is $\hat{y}_i$, which ranges from 0 to 1. Finally, a segmented image is reconstructed by the predicted value.

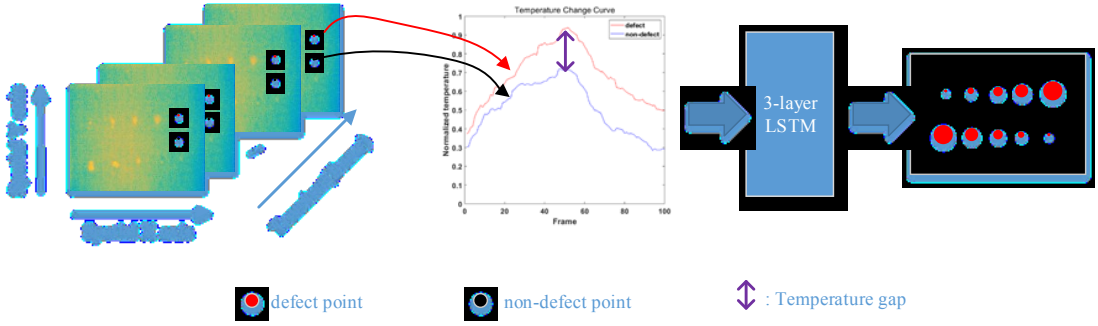

Fig.6. Sequence model prediction principle based on differential temperature signal vs. time at surface points corresponding to defective and sound areas.

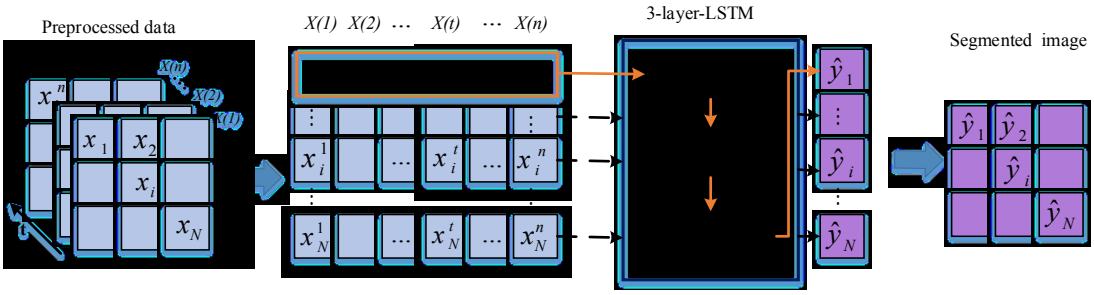

Fig.7. The process of 3-layer LSTM segmentation

For the data process, an important step is that all the defect pixels and the same number of non-defective pixels are selected for training. Note that the sequence data is already removed the background and normalized and the training non-defective pixels are selected randomly. This is to deal with data imbalance problems where the defective pixel is much lower than the sound pixel. The time steps are [*t*-*n*, *t*+*n*-1], where *t* is the highest temperature time and n is a multiple of 50. The label of each pixel is still marked as 0 and 1, representing the non-defect and defect areas, respectively.

2.2.3 Cross network learning strategy and evaluation

For more complex test pieces, due to their special structure and more influence of heat diffusion, the single spatial-based segmentation model needs to be optimized. The training of the above models starts from the random initialization weights, and Unet has such an advantage on small data sets. However, for complex situations, Unet cannot learn sufficient features from small data sets. Thus, we explore the cross learning strategy of adding VGG-16 pre-trained weights in the encoder to help the model to better extract weak defect features from large amounts of thermal information. In the decoder stage, the skip-connection with high-resolution features is added to preserve the accuracy of original model for defect shape, size, and position. This cross learning model is shown in Fig.8.

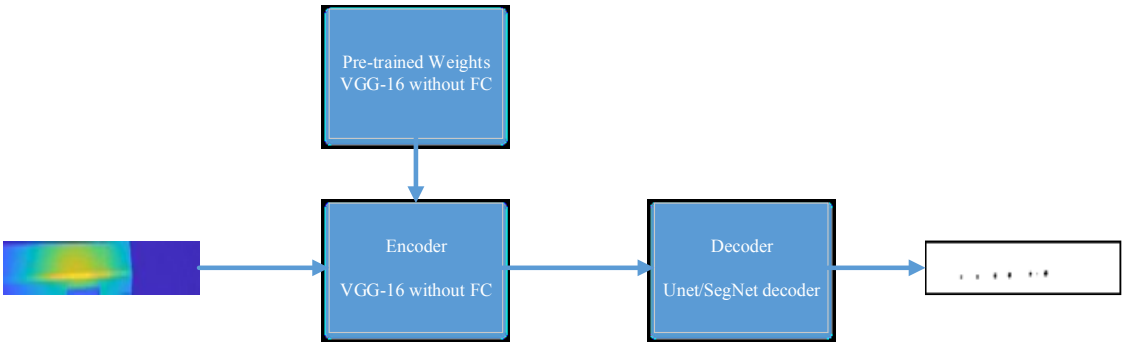

Fig.8. Cross learning of spatial-oriented model

For the detection of deeper defects, the spatial SNR value is very low, and it is necessary to use the information in the time domain to assist the spatial-oriented model to obtain the thermal characteristics of the defect. In this paper, PCA processing is performed on such specimens. Combined with the PCA extraction algorithm, The model can be regarded as a temporal-spatial model because PCA extracts several principal components from the thermal video with temporal-spatial features. The schematic is shown in Fig.9. The three-dimensional features including the temporal are compressed into the 2-D image, and then the spatial-oriented model is used to detect the defects.

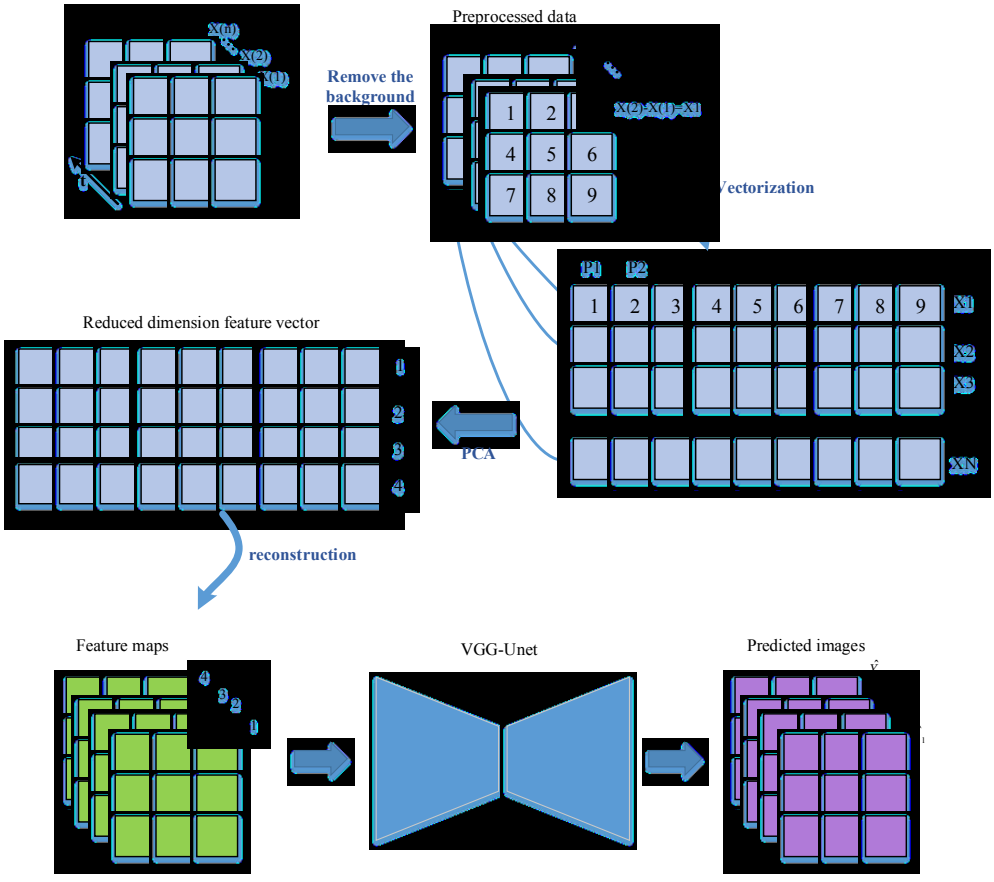

Fig.9. Feature extraction temporal-spatial model

Therefore, cross network learning strategy and evaluation will be fully validated as shown in Fig.10. The blue arrow in the figure shows the flow chart of comparing the segmentation effects of different models on different defect types. In this process, four different types of defect images are first augmented by rotation, color conversion, translation, etc., and then are segmented by different segmentation networks. POD will be used to evaluate the detection effects of different models. If the number of defects detected in the segmentation result is

significantly too low (for example, TP<2), the PCA or other processing will be introduced on the original sequence to extract the features, and then the segmentation network is applied to obtain the detection results. This process is shown by the yellow arrow.

In time domain, a 3-layer long short term memory (3-layer LSTM) loop is used to predict the pixels of different types of data. The process is shown by the red arrow.

In order to compare the detection effects of a model more clearly, criterion probability of detection (POD) [39][40] is selected. It is defined as (9)

$$POD=\frac{TP}{TP+FN} \tag{9}$$

where TP is true positive, indicating the number of defects detected, and FN is false negative, indicating the number of defects not detected.

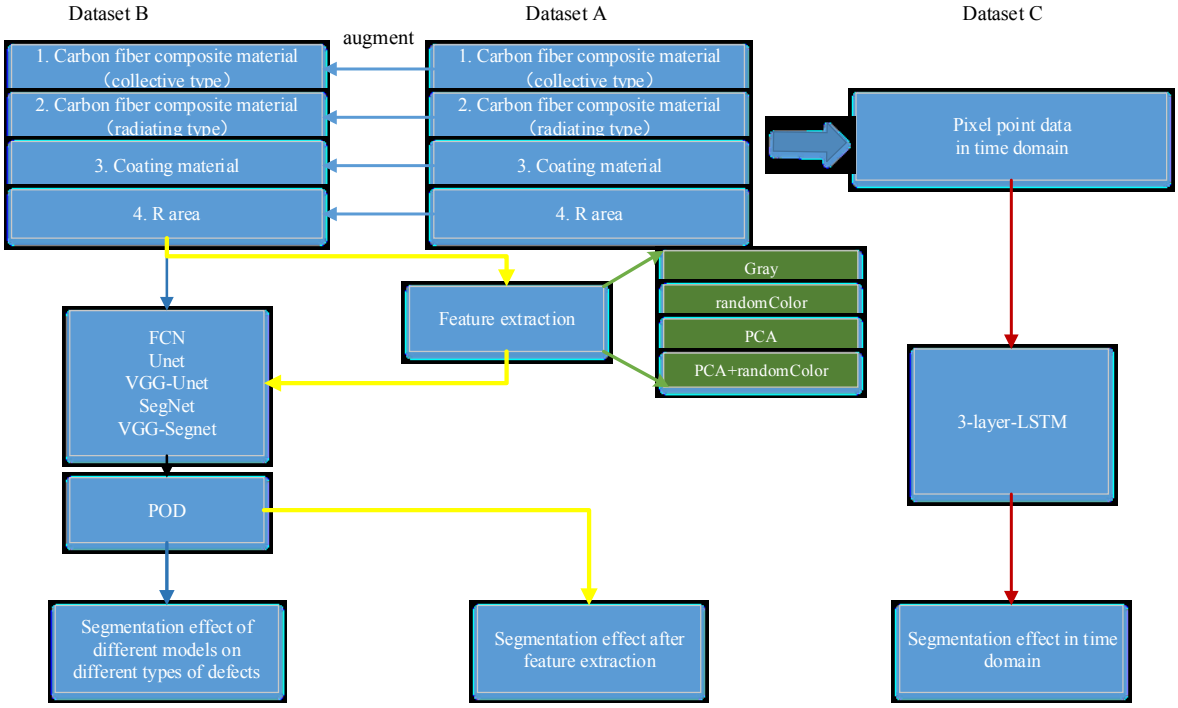

Fig.10. Cross network learning strategy and evaluation

3 Result and Discussion

3.1 Experiment Platform and Sample Preparation

The platform used to acquire the data is optical pulsed thermography including optical excitation source, two halogen lamps with a power of 2 kW in total, IR camera, PC, and the sample, as shown in Fig.11. The infrared thermal camera is FLIR A655sc, with the band is 7.5-14um, the temperature sensitivity is 0.05°C, and the maximum resolution is 640×480.

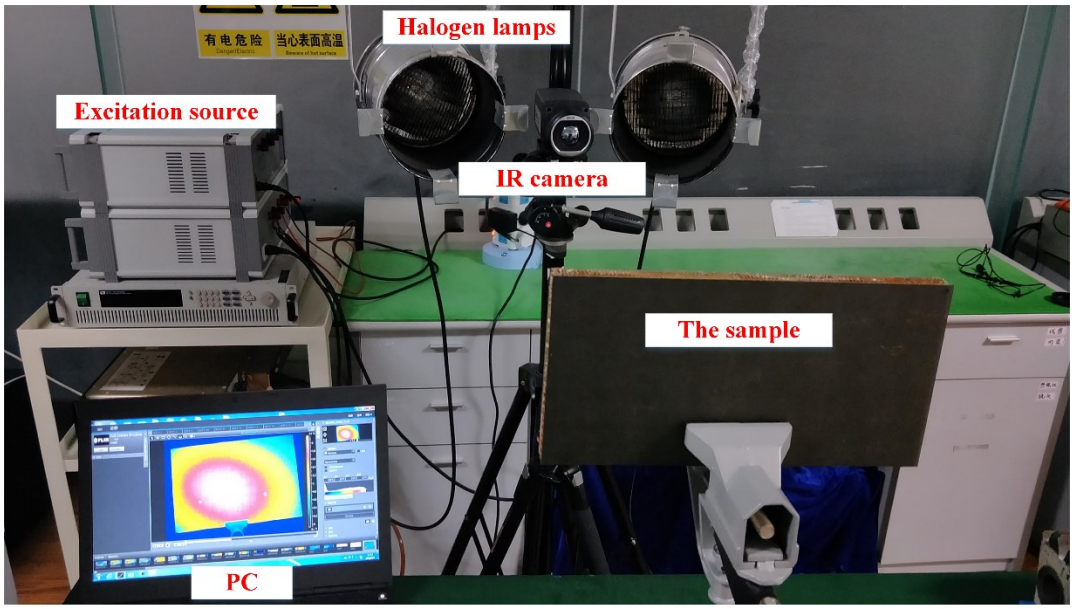

Fig.11. Experiment platform

Nine different samples tested in this paper are shown in Table 1. Eight of them are collective heat type samples, the last one is carbon fiber reinforced plastic (CFRP) with insulated heat type. Among the first 8 specimens, the No.1 is a carbon fiber composite with 16 sub-surface debond defects of different sizes. The No. 2 to No. 4 samples are coating materials with debond defects, and the No. 3 is a curved surface, which is more difficult to detect than No. 2. The samples No. 5 to No. 8 are CFRP with curved shape which named R area. There are debond defects at elbow, which is more challenging to detect.

Table 1. The description of different samples

Types	Samples	Indication	Dimension (mm)	Defect information(mm)	Picture
CFRP (collective heat type)	1	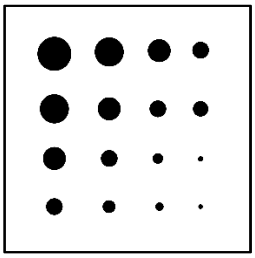	250×250×2.2	Depth: 2 or 2.2 Diameter: 2,4,6,8,10,12,16,20	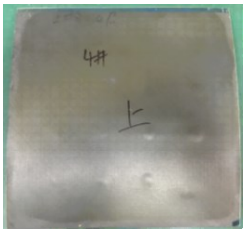
Coating material	2	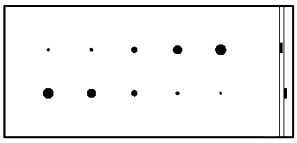	150×300×2	Depth: 1 or 1.2 Diameter: 3,5,7,10,12	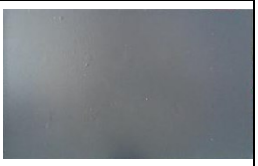
	3	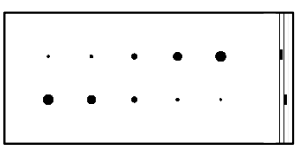	150×300×2	Depth: 1 or 1.2 Diameter: 3,5,7,10,12 curve	

	4	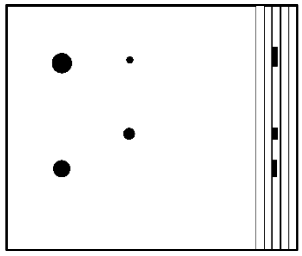	150×150×2	Depth:1.2 Diameter: 3,5,7,10	
R shape	5		100×100×8	Depth:1 to 1.5 Diameter: 9,10	
	6		100×100×8	Depth:1 to 1.5 Diameter: 9,10	
	7		100×100×8	Depth:1 to 1.5 Diameter: 6,8	
	8		100×100×8	Depth:1 to 1.5 Diameter: 6,8	
CFRP (radiant heat type)	9	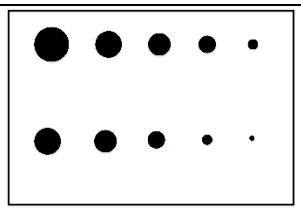	250×300×24.2	Depth: 2 or 2.2 Diameter: 3,6,10,14,18	

In order to verify the robustness of the model under the different experimental conditions, specimens in table 2 were detected using a portable optical pulsed thermography (POPT) system. No.10 and No.11 are R shape specimens of different diameters. No.12 is a flat bottom hole specimen. POPT system is shown in Fig.11, including an excitation source and CPU, a display screen, a halogen lamp with a power of 800 W, an IR camera and a grip, as shown in Fig.12. The infrared thermal camera is MAGNITY MAG-62, the temperature sensitivity is 0.06°C, and the resolution is 640×480.

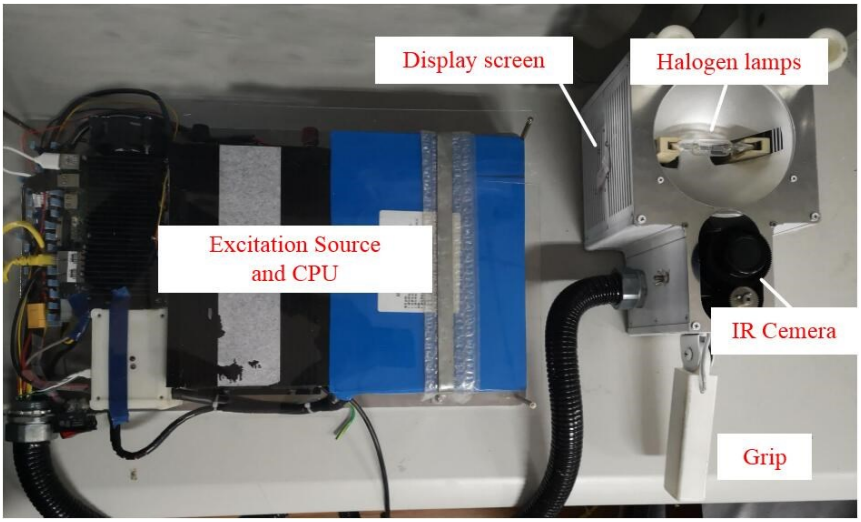

Fig.12. Portable optical pulsed thermography system

Table 2. The description of different samples tested by POPT

Types	Samples	Indication	Dimension (mm)	Defect information(mm)	Picture
R shape	10		100×100×8	Depth:1 to 1.5 Diameter: 9, 10	
	11		100×100×8	Depth:1 to 1.5 Diameter: 6, 8	
CFRP (collective heat type)	12	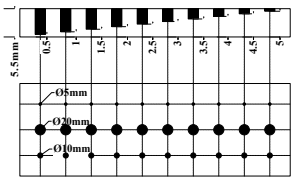	530×180×5.5	Depth:0.5, 1, 1.5, 2, 2.5, 3, 3.5, 4, 4.5, 5 Diameter: 5, 20, 10	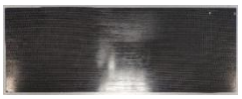

3.2 Result Analysis

In order to compare the detection effects of different segmentation models, different samples and different pretreatments, the following six models will be applied, namely Unet, VGG-Unet, Segnet, VGG-Segnet, FCN8, and 3-layer-LSTM. The detection results of the six models were compared for different data sets. It should be noted that all these models predict defects in the spatial domain, except that the 3-layer LSTM is in temporal.

3.2.1 Segmentation effect of different models on different type of defects

Table 3 shows the visual results of spatial models for flat or curved samples, while Table 4 shows the results of R shaped sample. It can be seen that the five segmentation models can better segment the defect information of CFRP and coating materials. Compared with the other models, the boundary of Unet segmentation is obvious bigger than the actual defect. VGG-Unet, Segnet, VGG-Segnet have a good performance for the segmentation results of the R shaped sample, while the defects with a diameter of 3mm in the curved coating material cannot be detected. FCN8 excels in coating materials but does not perform well in the R shaped sample. Table 5 shows the POD of those different models. It can be seen that, from the point of view of the detection rate, the detection effect of VGG-Unet is more remarkable for R shaped sample while Unet is for plat simple samples.

Table 3. Results comparison of spatial models for flat or curved samples

	original image	ground truth	Unet	VGG-Unet	Segnet	VGG-Segnet	FCN8
1	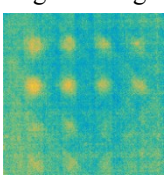	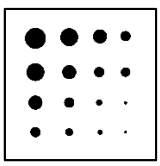	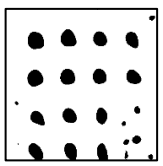	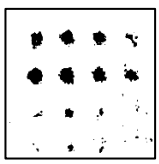	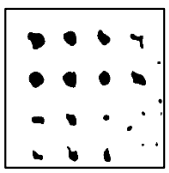	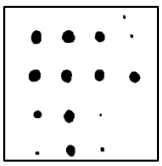	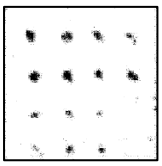
2	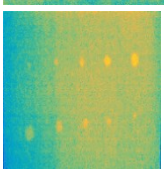	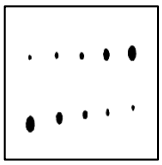	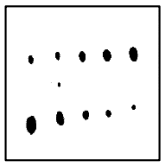	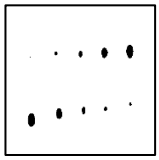	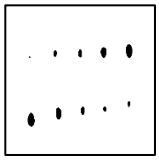	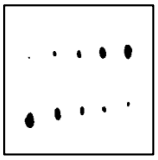	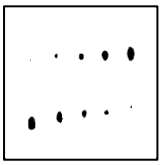

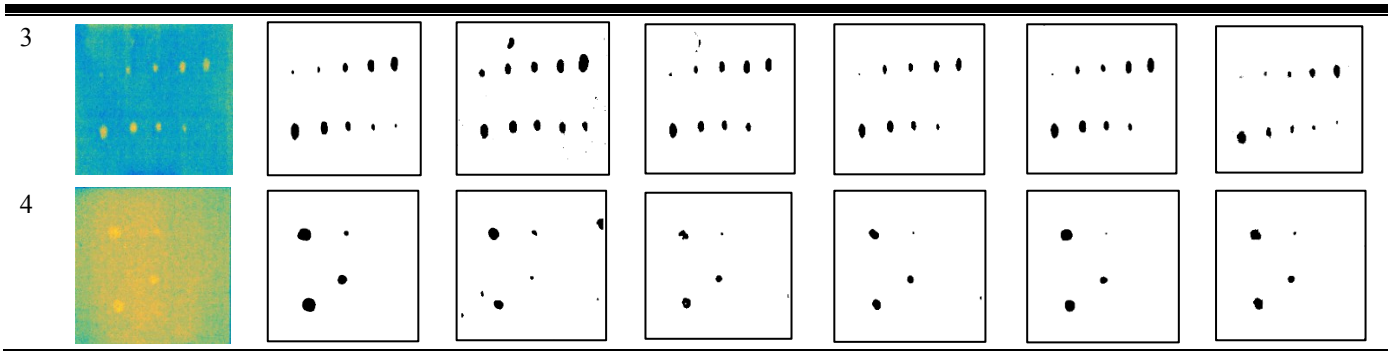

Table 4. Results comparison of spatial models for R area

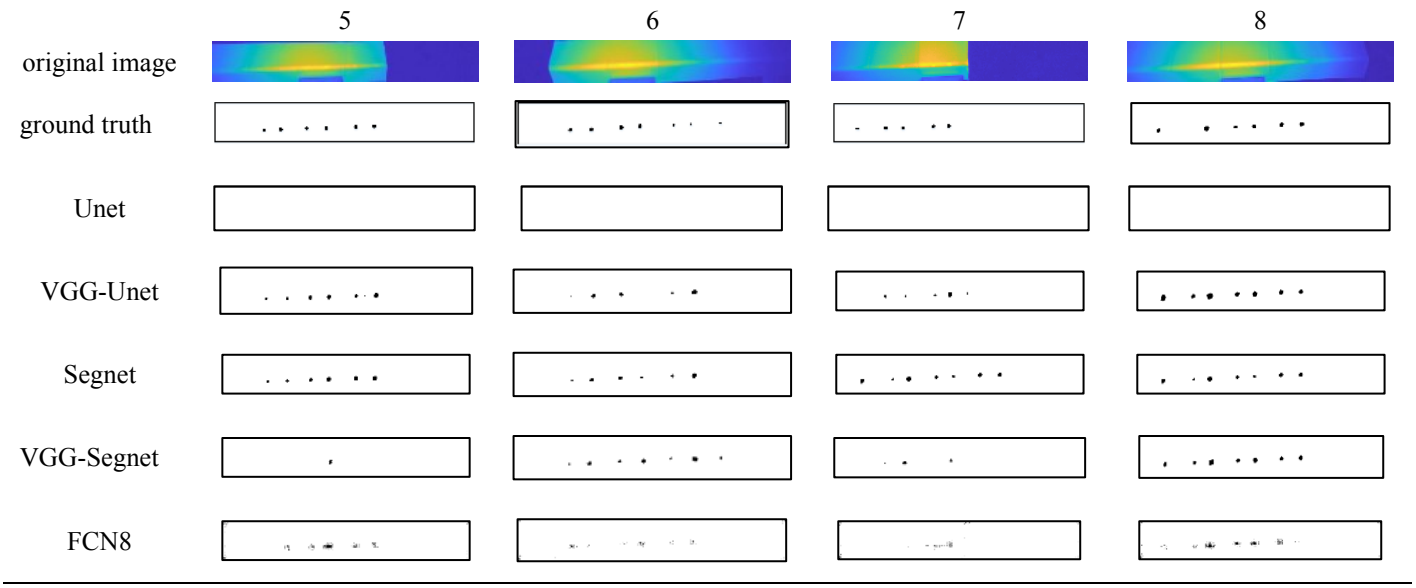

Table 5. Performance comparison of POD in spatial models

Samples	evaluation	Models				
		Unet	**VGG-Unet**	**Segnet**	**VGG-Segnet**	**FCN8**
1	TP	16	14	15	14	14
	FN	0	2	1	2	2
	POD	1.000	0.875	0.938	0.875	0.875
2	TP	10	9	10	10	10
	FN	0	1	0	0	0
	POD	1.000	0.900	1.000	1.000	1.000
3	TP	10	9	8	9	9
	FN	0	1	2	1	1
	POD	1.000	0.900	0.800	0.900	0.900
4	TP	4	4	3	4	4
	FN	0	0	1	0	0
	POD	1.000	1.000	0.750	1.000	1.000
5	TP	0	5	6	1	5
	FN	6	1	0	5	1

	POD	0	0.833	1.000	0.167	0.833
	TP	0	6	6	7	5
6	FN	7	1	1	0	2
	POD	0	0.857	0.857	1.000	0.714
	TP	0	5	4	3	1
7	FN	5	0	1	2	4
	POD	0	1.000	0.800	0.600	0.200
	TP	0	7	7	3	1
8	FN	7	0	0	4	6
	POD	0	1.000	1.000	0.429	0.143
Average	POD	0.571	0.921	0.893	0.746	0.708

The data obtained by POPT is segmented by the proposed model and the results are shown in Tabel 6**.** VGG-Unet can segment the two defects of the sample 10, while the segmentation effect of other models is greatly affected by the hot zone and the result is not good. Two-thirds of the defects in sample 11 can be segmented by VGG-Unet, while there exists partial errors. For the flat sample 12, VGG-Unet can segment one-third of the defects, and the segmentation effect is weaker than Unet. Under the condition of POPT experiment, the POD value of segmentation effect is shown in Table 7. Compared with other models, VGG-Unet has the highest average POD value, which can reach 0.667.

Table 6. Results comparison of spatial models for POPT

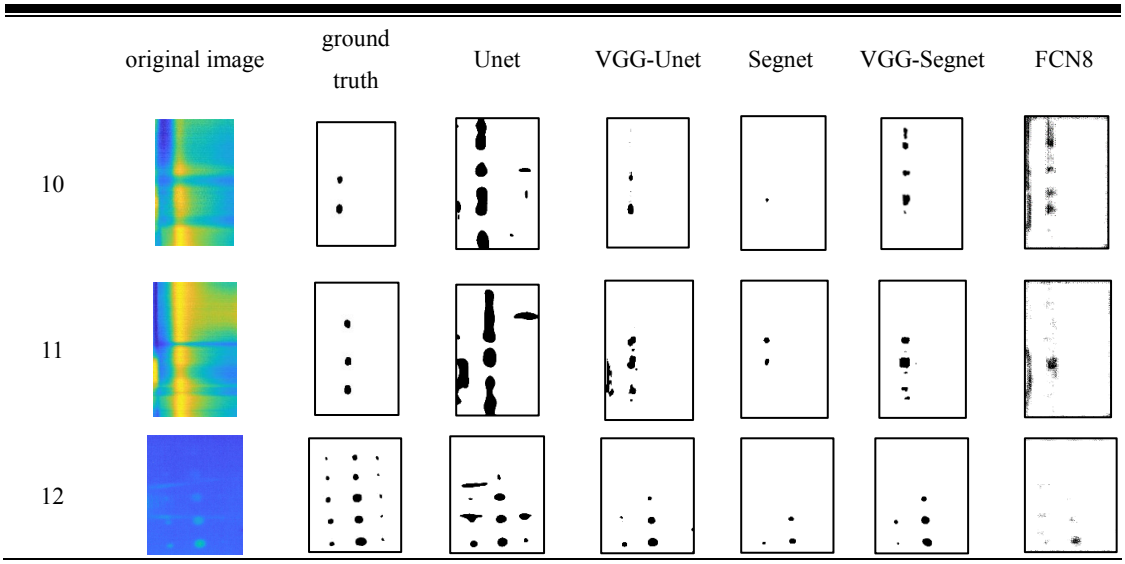

Table 7. Performance comparison of POD in spatial models for POPT

sample	Model				
	Unet	VGG-Unet	Segnet	VGG-Segnet	FCN8
1	0	1	0.5	0.5	0.5
2	0	0.667	0.333	0.667	0.333
3	0.6	0.333	0.2	0.333	0.067

Average	0.2	0.667	0.344	0.5	0.3

In summary, VGG-Unet can achieve good results in both high-power and low-power optical pulsed thermography platforms. The proposed mode has the capability of the robustness validation.

Previous models only predicted defects in the spatial domain. Using OPT to detect defects is based on the principle of heat conduction in the specimen, which is a process of transient. Thus, 3-layer-LSTM is applied to conduct the prediction of the transient characteristic. The results of each samples are shown in Table 8. Unfortunately, this model can detect defects well for coating materials and heat-collecting CFPR materials whereas it is almost impossible to detect for R shaped sample and heat-dissipating CFPR materials. The POD of this model is shown in Table 9.

Table 8. Results of 3-layer-LSTM

samples	1	2	3	4	5
3LSTM	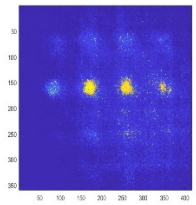	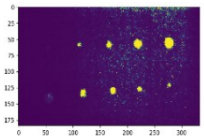	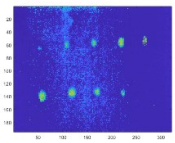	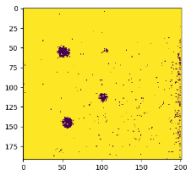	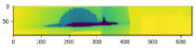
samples	6	7	8	9	
3LSTM	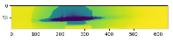	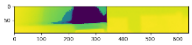	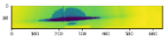	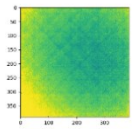	

Table 9. POD of 3-layer-LSTM

Model	**evaluation**	Samples								
		1	2	3	4	5	6	7	8	9
3-layer-LSTM	POD	0.625	0.900	0.900	1.000	0	0	0	0	0

3.2.2 Segmentation effect after feature extraction

For the sample 9, the SNR of the original image is very low due to the influence of the ambient halo and the depth of defect. As show in Fig.13, the most of the defect information is drowned in the hot zone of the specimen. The model can hardly segment the defect information from the original image.

In order to compare the segmentation effect of the model after different preprocessing methods, four methods are selected: Grayscale, randomColor, PCA, PCA+randomColor. After pre-processing, the segmentation results have been significantly improved. In particular, after PCA processing, the model can almost completely segment the defects. This is because the PCA compresses the information in the time domain first, and then the model extracts the information of the space. This method can enhance time domain and spatial information in the same time. The detailed results are shown in Table 10. The POD of samples after feature extraction can be found in Table 11.

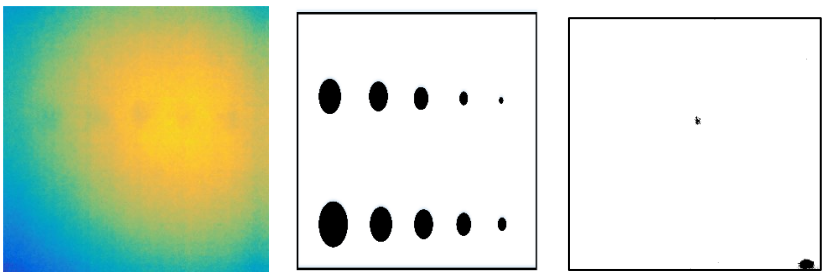

(a) original image (b) ground truth (c) segmentation result

Fig.13. The original image, ground truth and segmentation result of sample 9

Table 10. Segmentation effect after feature extraction of sample 9

Method	Gray	randomColor	PCA	PCA +randomColor
Feature map	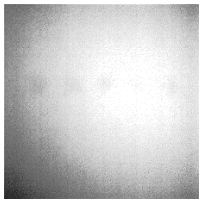		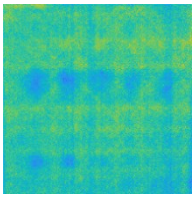	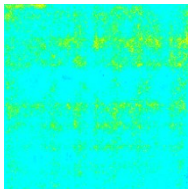
Result	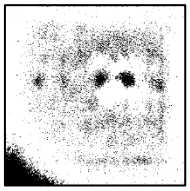	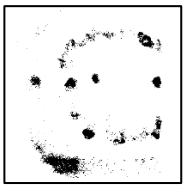	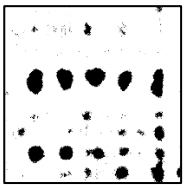	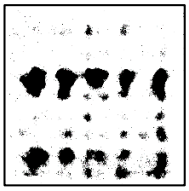

Table 11. POD after feature extraction

sample	Methods				
	origin	Gray	randomColor	PCA	PCA +randomColor
1	0.875	0.875	1	0.875	1
2	0.9	1	1	1	1
3	0.9	0.9	0.9	1	0.9
4	1	1	1	1	1
9	0	0.500	0.500	0.900	0.900
Average	0.735	0.855	0.880	0.955	0.960

4 Conclusion and Future Works

In this paper, deep cross learning strategy based segmentation models are applied in defect detection of composite materials. The validation results on four different type of specimen with different defects depth and diameter are discussed in a complete way. Cross learning strategy of VGG-Unet can basically reach the better performance in the spatial-oriented model. Because it combines the characteristics of Unet for small sample set segmentation and VGG pre-training weights. The 3-layer-LSTM for predicting defect information by temporal changes in the transient response of image pixels is not performing well in the R shaped sample. It is worth noting that after extracting certain features from low SNR images, especially of combining transient and spatial information, better evaluation results can be obtained. It is confirmed that the performance will be better as the training sets have the same type of data in the test sets. Future research will focus on the structured learning combination of transient and spatial information.

Acknowledgement

The work was supported by National Natural Science Foundation of China (No. 61971093). The work was supported by Science and Technology Department of Sichuan, China (Grant No.2019YJ0208, Grant No.2018JY0655).

References

[1] Miller F P, Vandome A F, Mcbrewster J. Carbon Fiber-Reinforced Polymer[M]. Alphascript Publishing, 2011.
[2] Bison P G, Grinzato E G, Vavilov V P. Inspecting thermal barrier coatings by IR thermography[J]. Proceedings of SPIE - The International Society for Optical Engineering, 2003, 5073(1):318-327.
[3] Chulkov A O, Vavilov V P. Hardware and Software for Thermal Nondestructive Testing of Metallic and Composite Materials[C]// 2016:1392–1397.
[4] Marinetti S, Grinzato E, Bison P G, *et al*. Statistical analysis of IR thermographic sequences by PCA[J]. Infrared Physics & Technology, 2004, 46(1–2):85-91.
[5] Rajic N. Principal component thermography for flaw contrast enhancement and flaw depth characterisation in composite structures[J]. Composite Structures, 2002, 58(4):521-528.
[6] Shepard S M, Beemer M F. Advances in thermographic signal reconstruction[C] //Thermosense: Thermal Infrared Applications XXXVII. International Society for Optics and Photonics, 2015, 9485: 94850R
[7] Hajrya R, Mechbal N, Vergé M. Damage Detection of Composite Structure Using Independent Component Analysis[C]// International Workshop on Structural Health Monitoring. 2011:241-248.
[8] Cheng L, Gao B, Tian G Y, *et al*. Impact Damage Detection and Identification Using Eddy Current Pulsed Thermography Through Integration of PCA and ICA[J]. IEEE Sensors Journal, 2014, 14(5):1655-1663.
[9] Maldague X, Marinetti S. Pulse phase infrared thermography[J]. Journal of Applied Physics, 1996, 79(5):2694-2698.
[10] Ibarra-Castanedo C, Maldague X P V. Interactive Methodology for Optimized Defect Characterization by Quantitative Pulsed Phase Thermography[J]. Research in Nondestructive Evaluation, 2005, 16(4):175-193.

[11] Gao B, Lu P, Woo W L, *et al*. Variational Bayesian Subgroup Adaptive Sparse Component Extraction for Diagnostic Imaging System[J]. IEEE Transactions on Industrial Electronics, 2018, 65(10):8142-8152.
[12] Lu P, Gao B, Feng Q, *et al*. Ensemble Variational Bayes Tensor Factorization for Super Resolution of CFRP Debond Detection[J]. Infrared Physics & Technology, 2017, 85:335–346.
[13] Lu P, Gao B, Woo W L, *et al*. Automatic Relevance Determination of Adaptive Variational Bayes Sparse Decomposition for Micro-Cracks Detection in Thermal Sensing[J]. IEEE Sensors Journal, 2017, 17(16): 5220-5230.
[14] Pilla M, Klein M, Maldague X, *et al*. New absolute contrast for pulsed thermography[J]. Quantitative Infrared Thermography Journal, 2002.
[15] Vavilov V P, Shiryaev V V, Chulkov A O. A novel data processing algorithm in thermal property measurement and defect detection by using one-sided active infrared thermography[C]. SPIE Sensing Technology + Applications. 2015:94850V.
[16] Zheng K , Chang Y S , Wang K H , *et al.* Improved non-destructive testing of carbon fiber reinforced polymer (CFRP) composites using pulsed thermograph[J]. Polymer Testing, 2015, 46:26-32.
[17] Zheng K , Chang Y S , Yao Y . Defect detection in CFRP structures using pulsed thermographic data enhanced by penalized least squares methods[J]. Composites Part B: Engineering, 2015, 79:351-358.
[18] Wang J G , Cao Z D , Yang B H , *et al.* Non-destructive testing of CFRP using pulsed thermographic data enhanced by wavelet transform-based image denoising[C]// 2017 36th Chinese Control Conference (CCC). IEEE, 2017.
[19] Venegas P , Usamentiaga R , Perán J, *et al.* Advances in RGB Projection Technique for Thermographic NDT: Channels Selection Criteria and Visualization Improvement[J]. International Journal of Thermophysics, 2018, 39(8):95-.
[20] Wang J, Zhao C. Visual defect recognition and location for pulsed thermography images based on defect-background contrast analysis[C]//2018 33rd Youth Academic Annual Conference of Chinese Association of Automation (YAC). IEEE, 2018: 1106-1111.
[21] Liu Y, Liu K, Gao Z, *et al.* Non-destructive defect evaluation of polymer composites via thermographic data analysis: A manifold learning method[J]. Infrared Physics & Technology, 2019, 97: 300-308.
[22] Feng D, Shi W, Chen L, *et al*. Infrared image segmentation with 2-D maximum entropy method based on particle swarm optimization (PSO)[J]. Pattern Recognition Letters, 2005, 26(5):597-603.
[23] Mei L, Wu L D, Wang Y W. Image processing in pulse heating infrared nondestructive test[J]. journal of infrared and millimeter waves, 2002, 21(5): 372-376.
[24] Feng Q, Gao B, Lu P, *et al*. Automatic seeded region growing for thermography debonding detection of CFRP[J]. NDT & E International, 2018, 99: 36-49.
[25] Kante Murali, Rama Koti Reddy D.V.. Segmentation of Thermographic Sequences in Frequency Modulated Thermal Wave Imaging for NDE of GFRP[J]. Transactions of Nanjing University of Aeronautics and Astronautics,2018,35(02):226-235.
[26] Yousefi B , Sharifipour H M , Castanedo C I , *et al.* Automatic IRNDT inspection applying sparse PCA-based clustering[C]// 2017 IEEE 30th Canadian Conference on Electrical and Computer Engineering (CCECE). IEEE, 2017.
[27] Zheng K , Chang Y S , Wang K H , *et al.* Thermographic clustering analysis for defect detection in CFRP structures[J]. Polymer Testing, 2016, 49:73-81.
[28] Zheng K, Yao Y. Automatic defect detection based on segmentation of pulsed thermographic images[J]. Chemometrics and Intelligent Laboratory Systems, 2017, 162: 35-43.

[29] Gao B , Li X , Woo W L , *et al.* Physics-Based Image Segmentation Using First Order Statistical Properties and Genetic Algorithm for Inductive Thermography Imaging[J]. IEEE Transactions on Image Processing A Publication of the IEEE Signal Processing Society, 2018, 27(5):2160.
[30] K. Simonyan and A. Zisserman, "Very deep convolutional networks for large-scale image recognition," arXiv preprint arXiv:1409.1556, 2014.
[31] Long J, Shelhamer E, Darrell T. Fully convolutional networks for semantic segmentation[C]//Proceedings of the IEEE conference on computer vision and pattern recognition. 2015: 3431-3440.
[32] Badrinarayanan V, Kendall A, Cipolla R. Segnet: A deep convolutional encoder-decoder architecture for image segmentation[J]. IEEE transactions on pattern analysis and machine intelligence, 2017, 39(12): 2481-2495.
[33] Yu F, Koltun V. Multi-scale context aggregation by dilated convolutions[J]. arXiv preprint arXiv:1511.07122, 2015.
[34] Chen L C, Papandreou G, Kokkinos I, *et al*. DeepLab: Semantic Image Segmentation with Deep Convolutional Nets, Atrous Convolution, and Fully Connected CRFs[J]. arXiv preprint arXiv:1606.00915, 2016.
[35] Lin G, Milan A, Shen C, *et al*. RefineNet: Multi-path Refinement Networks for High-Resolution Semantic Segmentation[C]//Cvpr. 2017, 1(2): 5.
[36] He K, Zhang X, Ren S, *et al*. Deep residual learning for image recognition[C]//Proceedings of the IEEE conference on computer vision and pattern recognition. 2016: 770-778.
[37] Zhao H, Shi J, Qi X, *et al*. Pyramid scene parsing network[C]//IEEE Conf. on Computer Vision and Pattern Recognition (CVPR). 2017: 2881-2890.
[38] Ronneberger O, Fischer P, Brox T. U-Net: Convolutional Networks for Biomedical Image Segmentation[C]// International Conference on Medical Image Computing & Computer-assisted Intervention. 2015.
[39] Gao B, Woo W L, Tian G, *et al*. Unsupervised Diagnostic and Monitoring of Defects Using Waveguide Imaging with Adaptive Sparse Representation[J]. IEEE Trans. Industrial Informatics, 2016, 12(1): 405-416.
[40] Yunze He, Sheng Chen, Deqiang Zhou, Pan Wang, Shared Excitation Based Nonlinear Ultrasound and Vibrothermography Testing for CFRP Barely Visible Impact Damage Inspection, IEEE Transactions on Industrial Informatics, 2018, 14 (12), 5575-5584.